# THERMOMECHANICAL SENSITIVITY OF MICROCANTILEVER IN THE MID-INFRARED SPECTRAL REGION

BY

BEOMJIN KWON

THESIS

Submitted in partial fulfillment of the requirements
for the degree of Master of Science in Mechanical Engineering
in the Graduate College of the
University of Illinois at Urbana-Champaign, 2009

Urbana, Illinois

Adviser:

Associate Professor William P. King

# ABSTRACT

This paper reports the thermomechanical sensitivity of bimaterial cantilevers over a mid-infrared (IR) spectral range (5-10 μm) that is critical both for chemical analysis via vibrational spectroscopy and for direct thermal detection in the 300-700 K range. Mechanical bending sensitivity and noise were measured and modeled for six commercially available microcantilevers, which consist of either an aluminum film on a silicon cantilever or a gold film on a silicon nitride cantilever. The spectral sensitivity of each cantilever was determined by recording cantilever deflection when illuminated with IR light from a monochromator. Rigorous modeling and systematic characterization of the optical system allowed for a quantitative estimate of IR energy incident upon the cantilever. Separately, spectral absorptance of the cantilever was measured using Fourier transform infrared (FT-IR) microscopy, which was compared with analytical models of radiation onto the cantilever and heat flow within the cantilever. The predictions of microcantilever thermomechanical bending sensitivity and noise agree well with measurements, resulting in a ranking of these cantilevers for their potential use in IR measurements.

# ACKNOWLEDGMENTS

I would like to thank Prof. William P. King for guiding and supporting my research with mentorship and encouragement throughout my studies at University of Illinois at Urbana-Champaign. I am also grateful to Prof. Rohit Bhargava for letting me use his laboratory equipments and providing valuable advices on my research. It was great pleasure to discuss about overall research with Prof. Keunhan Park.

I deeply appreciate Cheng Wang for working together on designing experimental setup. Thank you, Dr. Matthew Schulmerich and Dr. Michael Walsh, who have helped me taking spectrum using FT-IR spectrometers.

Finally, I would like to acknowledge my family for endless love, sacrifices and prayers.

# TABLE OF CONTENTS

# List of Tables

# List of Figures

# CHATPER 1

# INTRODUCTION

The bending of a bilayered or multilayered cantilever can be used to measure small temperature changes or heat flows.[1,2] Infrared (IR) measurements with bimaterial microcantilevers have shown a temperature sensitivity down to $10^{-5}$ K and heat flow measurements as small as 10 fJ.[3,4] These thermal characteristics can be used to analyze the properties of samples down to nanogram quantities, compared to milligrams or larger in conventional instruments.[5] Applications of microcantilevers for IR measurements also include chemical detection using vibrational spectroscopic response of materials, for example, in pharmaceuticals analysis.[6,7] In particular, an attractive feature of measurements using microcantilevers is that they do not need cryogenic cooling for eliminating thermal noise in spectroscopic applications.[4] Further, the intrinsically small sampling volume and commercial availability of cantilevers makes them very attractive as detectors for measuring spectra from microscopic regions.

Published works on IR spectroscopy using bimaterial microcantilevers report measurements on biological species,[5,6,8] chemicals,[3,9] and explosives.[7,10] While offering impressive potential for this technology, however, the quality of spectroscopic data lags traditional IR microspectroscopic methods.[11] Further, spectral concordance between cantilever-based measurements and conventional microspectroscopies has not been excellent. It was noted specifically that some spectral peaks can be missing and relative peak intensities were not identical. This discordance is undesirable as a good match between measured spectra and

reference library spectra is often required for analytical tasks. Consequently, despite the demonstrated potential, the utility of cantilever-based approaches for routine spectroscopic analyses is ultimately limited. To understand spectral data acquisition using microcantilever sensors, it is important to understand the IR spectral response of these structures. Cantilever characterization, however, is tightly coupled to the optical system used. Hence, there is a need to characterize the spectral response of cantilevers while characterizing the optical setup used for the same. To our knowledge, there are no published reports on determining the IR spectral characteristics of microcantilevers.

Our aim in this study is to determine the IR spectral characteristics of commercially available microcantilevers. While some groups have custom-designed and fabricated bimaterial microcantilevers for IR measurements,[12-14] most published studies have used commercially available microcantilevers.[5-8,10] Hence, the results are directly relevant in both understanding presently available microcantilevers and measurements using the same as well as for future optimization of instruments using microcantilevers. To accomplish quantitative characterization, we also developed an analytical model for predicting spectral sensitivity and noise in bimaterial cantilevers. Our approach is based on previous works that predicted thermomechanical sensitivity and noise,[3,15-17] but expands it to include spectral characteristics of the cantilevers.

# CHAPTER 2

# MODELING CANTILEVER SENSITIVITY AND NOISE

The thermomechanical bending sensitivity of a microcantilever can be estimated from incident IR radiation, IR response characteristics of the cantilever, and the mechanical properties of the cantilever. For a beam consisting of two materials with different thermal expansion coefficients, the cantilever deflection can be expressed as[3,18]

$$\frac{d^2z}{dx^2} = 6(\alpha_s - \alpha_c)\left(\frac{t_s + t_c}{t_c{}^2 K}\right)[T(x) - T_0] \qquad (1)$$

where

$$K = 4 + 6\left(\frac{t_s}{t_c}\right) + 4\left(\frac{t_s}{t_c}\right)^2 + \frac{E_s}{E_c}\left(\frac{t_s}{t_c}\right)^3 + \frac{E_c}{E_S}\left(\frac{t_c}{t_s}\right),$$

$z(x)$ is the vertical deflection, $T(x)$-$T_0$ is the temperature difference between the cantilever and the ambient temperature at a location $x$ along its length, $\alpha$ is the thermal expansion coefficient, $t$ is the layer thickness with subscripts indicating the substrate ($s$) or the coating ($c$) material, and $E$ is Young's modulus. In order to obtain an analytical solution for the Eq. (1), several simplifications are employed in the heat transfer analysis. First, the incident radiation is assumed to be uniformly distributed over the cantilever area. Second, the Biot number is assumed to be less than one such that the temperature distribution within the cantilever is one-dimensional. The cantilever is assumed to lose heat along its length and due to thermal conduction to the air, where the effective heat transfer coefficient is $h$ = 1000 W/m$^2$-K.[19-21] Radiative heat loss from cantilever is assumed to be negligible as the cantilever is always near room temperature. With these assumptions and appropriate boundary conditions, the temperature distribution $T(x)$ can be

analytically described. Substituting $T(x)$ into Eq. (1) yields the following analytical solution of the cantilever deflection:

$$z(L) = 3(\alpha_s - \alpha_c)\left(\frac{t_s + t_c}{{t_c}^2 K}\right)\frac{P_\lambda}{(t_s + t_c + w)hL\beta^2}\left(\tanh(\beta L)\left(\sinh(\beta L) - \beta L\right) - \cosh(\beta L) + \frac{1}{2}\beta^2 L^2 + 1\right),$$

where

$$\beta = \sqrt{\frac{2(t_s + t_c + w)h}{(\gamma_s t_s + \gamma_c t_c)w}}, \tag{2}$$

$L$ is cantilever length, $w$ is cantilever width, $\gamma$ is the thermal conductivity of the cantilever, and $P_\lambda$ is the spectral radiant power absorbed by the cantilever. The thermomechanical sensitivity of the cantilever, defined as angular displacement per unit spectral radiant power absorbed at the free end is

$$S = \frac{1}{P_\lambda}\cdot\left.\frac{dz}{dx}\right|_{x=L} = 3(\alpha_s - \alpha_c)\left(\frac{t_s + t_c}{{t_c}^2 K}\right)\frac{1}{(t_s + t_c + w)hL}\left(L - \frac{\tanh(\beta L)}{\beta}\right). \tag{3}$$

While the above analysis provides a measure of sensitivity, noise of the cantilever must also be considered. In general, measurements of noise include contributions from intrinsic factors such as thermomechanical noise and temperature fluctuations, and extrinsic factors such as environmental vibration and instrument noise.[22] Here, we consider only thermomechanical noise as it has been reported to be two orders of magnitude larger than the noise due to temperature fluctuations for small quality factor ($Q$~100) microcantilevers.[15] Thermomechanical noise can be predicted from a continuous energy transformation between stored mechanical energy in the cantilever and thermal energy of the environment.[15] This energy conversion induces the thermal vibration of the cantilever, whose amplitude can be predicted using the equipartition theorem.[23] When the measurement bandwidth ($B$) is selected and the quality factor of the microcantilever

($Q$) is measured, the root-mean-square (rms) displacement of the cantilever tip ($\delta z_{th}$) due to thermomechanical noise is predicted to be[15]

$$\sqrt{\left\langle \delta z_{th}^{\,2} \right\rangle} = \sqrt{\frac{4k_B TB}{Qk\omega_0}} \,. \tag{4}$$

where $k_B$ is Boltzmann's constant, $T$ is absolute temperature, $k$ is cantilever spring constant, and $\omega_0$ is mechanical resonance frequency of microcantilever. This relation is established for a rectangular cantilever.

We evaluated the deflection sensitivity and signal to noise ratio (SNR) of 73 bimaterial microcantilevers available from the following vendors: MikroMasch, NanoAndMore, Nanosensors, and Veeco Probes. In order to search those appropriate for thermomechanical deflection measurements, cantilevers possessing a nominal spring constant outside the range of $0.01 < k < 1$ N/m were not included.[10] For very stiff cantilevers, the cantilever will not bend much upon heating. For very soft cantilevers, thermomechanical noise will cause the cantilever to be unstable and unsuitable for bending measurements. For cantilevers having an appropriate nominal stiffness, the thermomechanical deflection sensitivity is predicted by using Eq. (3) and the analytical SNR was obtained from the ratio of the theoretical deflection predicted by Eq. (2) to the theoretical noise predicted by Eq. (4). Based on this initial screening, we selected six cantilevers having different combinations of deflection sensitivity and SNR.

Table 1 lists each of the selected cantilever's name, manufacturer, material composition and dimensions. Figure 1 shows the cantilever shapes and critical dimensions. All of the cantilever types in this study are V-shaped, except for Type B which is rectangular. A V-shaped cantilever can be approximated to be an equivalent rectangular cantilever of length $L_1$ and width $2\overline{d}$ from the parallel beam approximation, which allows the use of Eq. (2) through (4).[24] Table 2 compares

the predicted and measured deflection and SNR of the six microcantilevers for an incident wavelength of 7.5 μm.

# CHAPTER 3

# EXPERIMENTAL SETUP AND EXPERIMENTS

Figure 2 shows the experimental setup for cantilever characterization. An optical chopper modulates broad band light emitted from an IR emitter operating at 1100 K at $f_0$ = 380 Hz. The selection of the modulation frequency is limited by three factors: 60 Hz electrical noise, $1/f$ electrical noise, and the beam modulation attenuation. Thus, the modulation frequency is selected to exclude multiples of 60 Hz, above 100 Hz where the $1/f$ electrical noise dominates, and over 400 Hz where beam attenuation is significant. The modulated light transmits through a monochromator that generates a spectrally narrowband beam with the bandwidth of 100 nm in the 5-10 μm range. The monochromator is an Oriel 260 ¼ m monochromator equipped with a single grating of blaze wavelength optimized for 7 μm and a line density of 75 lines/mm. Light exiting the monochromator is focused onto a cantilever via a concave reflector. The beam heats the bimaterial cantilever at the modulated frequency and, in turn, induces thermomechanical deflection at the same frequency. The frequency of the modulated light has been set to be much smaller than the inverse of the thermal time constant and also to be much smaller than the mechanical resonance frequency, such that the cantilever deflection corresponds to the incident IR radiation alone. The amplitude of the cantilever deflection is measured by an optical quad-cell readout system of the AFM. The AFM optical readout output voltage is processed with a spectrum analyzer with an integration bandwidth of 1 Hz and integration time of 20.48 s.

In order to quantify the IR radiation incident upon the cantilever, the spectral efficiency of the monochromator ($\eta_{\lambda_M}$) was estimated using a Bruker Vertex 70 Fourier-transform infrared

(FT-IR) spectrometer. Spectra were acquired over the mid-IR range at an undersampling ratio of 2 referenced to the He-Ne laser to provide a free scanning spectral range of 7200-0 $cm^{-1}$. Interferograms were acquired at a nominal resolution of 4 $cm^{-1}$, signal averaged using 32 scans and fast Fourier-transformed using triangular apodization. The radiant power at each monochromator wavelength ($\dot{Q}_{\lambda_{MO}}$) was obtained from the spectrum, which was then divided by the predicted monochromator input radiant power to estimate the $\eta_{\lambda_M}$ as $\eta_{\lambda_M} = \dot{Q}_{\lambda_{MO}} / \varepsilon_{\lambda_E} I_{b_{\lambda_E}} A_E F_{EM} \eta_m$, where $\varepsilon_{\lambda_E}$ is the emissivity of the IR emitter, $I_{b\lambda E}$ is the spectral blackbody intensity of the IR emitter, $A_E$ is the surface area of the IR emitter, $F_{EM}$ is the view factor from the light source to the mirror within the IR emitter,[25] and $\eta_m$ is the mirror reflectance. Figure 3 presents the monochromator spectral efficiency $\eta_{\lambda_M}$ as a function of wavelength. Generally, $\eta_{\lambda_M}$ increases with wavelength in given spectral range in spite of the fact that the blaze wavelength of the grating is 7 μm. Above the blaze wavelength, the second and third order effect of the grating becomes notable, as the grating efficiency starts to increase significantly from the half the blaze wavelength (3.5 μm) according to the manufacturer's data sheet. This multiple order radiations of the grating enlarge the magnitude of $\dot{Q}_{\lambda_{MO}}$ and, in turn, result in high $\eta_{\lambda_M}$ above the blaze wavelength.

Separately, the cantilever IR characteristics were measured using a Perkin-Elmer Spotlight 400 FT-IR imaging system, which consists of a rapid-scan spectrometer coupled to a microscope equipped with a linear array detector. Transmittance and reflectance examinations of bimaterial cantilevers were recorded over the 7200-0 $cm^{-1}$ range and a range of 3000–704 $cm^{-1}$ (or 3.33-14.2 μm) was saved for analysis. Spectral transmittance was obtained from the ratio of the transmission intensity of the cantilever by the reference intensity of air. Similarly, reflectance

was measured from the ratio of the reflection intensity of cantilever surface to the reference intensity of a gold-coated glass slide. Then, the radiative energy balance for a transmitting layer is adopted to estimate absorbance at each wavelength which states that the sum of transmittance, reflectance, and absorptance is unity.[26] For each optical property and each cantilever, the infrared measurement was repeated over 32 times and averaged to minimize the uncertainties in measurements. As the width of the microcantilevers is tens of micrometers and the beam spot size of the spectrometer is 15×15 $\mu m^2$, diffractions plays a significant role in the measurements. Further measurement uncertainty may also arise from a tilt in the microcantilever when it is placed on the sample stage of the IR microscope. As shown in Figure 4 and reported by Wig and co-authors,[26] the absorption is dependent on the material composition and thicknesses of the layers of bimaterial microcantilevers. In Figure 4, higher thickness ratio of the two beam materials ($t_c$ / $t_s$) correlates with higher absorbance. The Au-$SiN_x$ cantilevers were observed to absorb nearly 50 % more than the Al-Si ones in this spectral region. As expected, material composition and thickness ratio between the substrate and the metal layers affect the IR absorption and present an opportunity to adjust for optimization of these cantilevers. Multiple small peaks in the spectra are likely due both to interference effect between the surfaces of the cantilever and scattering from the surface. Recently, detailed optical models for IR microscopy have been proposed, when allowing for rigorous modeling and predictions of scattering.[27,28] Hence, the results here are highly relevant for comparative analysis but absolute spectral behavior may require a further, small correction.

# CHAPTER 4

# RESULTS AND DISCUSSION

Bimaterial cantilever deflection was monitored by an AFM optical readout system and was proportionally translated into AFM output voltage. For the calibration of the cantilever detector deflection voltage to deflection distance, the deflection sensitivity of each cantilever was measured and multiplied with the AFM output voltage. Figure 5 shows measured cantilever deflection as a function of illuminating IR wavelength. The prediction for the deflection of the bimaterial cantilevers was calculated by using Eq. (2) with estimated spectral radiant power absorbed by the cantilever. The spectral radiant power absorbed by the cantilever is approximated to be the cumulative result of spectral blackbody intensity of the IR emitter, emissivity of the IR emitter, monochromator transmission efficiency and absorption characteristics of microcantilevers, which can be expressed as $P_\lambda = \dot{Q}_{\lambda_{MO}} \alpha_\lambda \, A_c / A_s$ , where $\alpha_\lambda$ is the spectral absorptance of the bimaterial cantilever, $A_c$ is the surface area of the cantilever, and $A_s$ is the beam focal spot area, which was estimated to be 250 mm$^2$.[4] The spot area is much larger than the cantilever area, but was constant for each measurement.

The overall amplitude of the thermomechanical deflection predicted by Eq. (2) agrees well with measurement, as does the spectral profile. Hence, Eq. (2) is useful for predicting photothermal sensitivities of the bimaterial cantilevers in the selected spectral region. However, spectra in Fig. 5 exhibit discrepancies in the spectral regions at 5-6.5 μm and 9-10 μm. We believe that the differences of these curves arise from atmospheric absorption from water vapor ($H_2O$) and carbon dioxide ($CO_2$). Specifically, the fundamental vibrational modes of $H_2O$ at 6.3

μm and $CO_2$ at 9.4 μm contribute to absorption that is apparent in single beam spectra.[29] In turn, the attenuation of the radiative energy into the cantilever possibly leads to a smaller thermomechanical deflection than the predicted deflection within these regions.[30]

Table 2 shows measured and predicted SNR values for an incident wavelength of 7.5 μm. The AFM optical readout voltage is affected by noise sources as described previously. The contribution of these noises was captured by performing a Fourier transform on the AFM output signal at the modulation frequency in the absence of IR incidence on the microcantilever. The data were recorded at the same integration bandwidth (1 Hz) and an integration time of 5 minutes. The magnitude of the noise was measured to be in the order of $10^{-6}$ – $10^{-5}$ V forming a baseline for the AFM output signal, which then corresponds to the thermomechanical deflection measurement baseline noise of 0.206 – 1.28 pm. We had previously hypothesized that thermomechanical noise was dominant for these measurements. Hence, thermomechanical noise of cantilever at off-resonance frequency was predicted by Eq. (4) and compared with the measured SNR. The predicted SNR is of the same order of magnitude as measured SNR except for type E and F cantilevers. These cantilevers also have the smallest thermomechanical deflections, suggesting that the proportional thermomechanical noise becomes lower and other sources become significant. Interestingly, cantilevers that undergo relatively larger thermomechanical deflections exhibit relatively higher SNR. We can surmise that the noise likely saturates at a certain level or grows much slower than the signal and is not simply proportional to the signal (deflection). The practical implication of this observation is that cantilever deflection alone does not predict SNR. Hence, in addition to materials and relative thickness of the two layers, as noted in the previous section, absolute deflection of the cantilever is likely to be another important parameter in designing optimal cantilevers for sensing.

# CHAPTER 5

# CONCLUSION

We have predicted thermomechanical sensitivity and noise for bimaterial microcantilevers over the IR region. The developed model was tested using six commercially available cantilevers over the wavelength range 5-10 μm, which is important for chemical analyses. An analytical model was established and the spectral absorptance of the cantilevers was measured using IR spectroscopy. The predictions of microcantilever thermomechanical bending sensitivity showed good agreement with measurements over 6.5-9 μm wavelengths where the atmospheric infrared absorption is weak. We also demonstrated that the thermomechanical noise was dominant in measurements and matched experimentally measured values. Together, the analytical model and measurements reported in this manuscript indicate the key design parameters for using biomaterial microcantilevers for spectral sensing in IR spectral region.

# REFERENCES


[1] S. Shen, A. Narayanaswamy, and G. Chen, Nano Lett. **9,** 2909 (2009).

[2] Y. De Wilde, F. Formanek, R. Carminati, B. Gralak, P. A. Lemoine, K. Joulain, J. P. Mulet, Y. Chen, and J. J. Greffet, Nature **444,** 740 (2006).

[3] J. R. Barnes, R. J. Stephenson, C. N. Woodburn, S. J. Oshea, M. E. Welland, T. Rayment, J. K. Gimzewski, and C. Gerber, Rev. Sci. Instrum. **65,** 3793 (1994).

[4] J. Varesi, J. Lai, T. Perazzo, Z. Shi, and A. Majumdar, Appl. Phys. Lett. **71,** 306 (1997).

[5] A. Wig, E. T. Arakawa, A. Passian, T. L. Ferrell, and T. Thundat, Sens. Actuators B: Chem. **114,** 206 (2006).

[6] E. T. Arakawa, N. V. Lavrik, and P. G. Datskos, Appl. Opt. **42,** 1757 (2003).

[7] C. W. Van Neste, L. R. Senesac, D. Yi, and T. Thundat, Appl. Phys. Lett. **92,** 134102 (2008).

[8] E. T. Arakawa, N. V. Lavrik, S. Rajic, and P. G. Datskos, Ultramicroscopy **97,** 459 (2003).

[9] P. G. Datskos, M. J. Sepaniak, C. A. Tipple, and N. Lavrik, Sens. Actuators B: Chem. **76,** 393 (2001).

[10] A. R. Krause, C. Van Neste, L. Senesac, T. Thundat, and E. Finot, J. Appl. Phys. **103,** 094906 (2008).

[11] I. W. Levin and R. Bhargava, Annu. Rev. Phys. Chem. **56,** 429 (2005).

[12] T. Perazzo, M. Mao, O. Kwon, A. Majumdar, J. B. Varesi, and P. Norton, Appl. Phys. Lett. **74,** 3567 (1999).

[13] D. Grbovic, N. V. Lavrik, P. G. Datskos, D. Forrai, E. Nelson, J. Devitt, and B. McIntyre, Appl. Phys. Lett. **89,** 073118 (2006).

[14] S. R. Hunter, R. A. Amantea, L. A. Goodman, D. B. Kharas, S. Gershtein, J. R. Matey, S. N. Perna, Y. Yu, N. Maley, and L. K. White, Proc. SPIE **5074,** 469 (2003).

[15] P. G. Datskos, N. V. Lavrik, and S. Rajic, Rev. Sci. Instrum. **75,** 1134 (2004).

[16] H. J. Butt and M. Jaschke, Nanotechnology **6,** 1-7 (1995).

[17] J. Lai, T. Perazzo, Z. Shi, and A. Majumdar, Sens. Actuators A: Phys. **58,** 113 (1997).

[18] R. J. Roark and W. C. Young, *Formulas for Stress and Strain*, 5th ed. (McGraw-Hill, New York, 1975).

[19] J. Lee, T. L. Wright, M. R. Abel, E. O. Sunden, A. Marchenkov, S. Graham, and W. P. King, J. Appl. Phys. **101,** 014906 (2007).

[20] K. J. Kim and W. P. King, Appl. Therm. Eng. **29,** 1631 (2009).

[21] K. Park, J. Lee, Z. M. M. Zhang, and W. P. King, J. MEMS **16,** 213 (2007).

[22] Z. Djuric, D. Randjelovic, I. Jokic, J. Matovic, and J. Lamovec, Infrared Phys. Tech. **50,** 51 (2007).

[23] H. J. Butt and M. Jaschke, Nanotechnology **6,** 1 (1995).

[24] J. E. Sader, Rev. Sci. Instrum. **66,** 4583 (1995).

[25] F. P. Incropera and D. P. Dewitt, *Fundamentals of heat and mass transfer*, 5th ed. (John Wiley & Sons, New Jersey, 2002).

[26] A. Wig, A. Passian, E. Arakawa, T. L. Ferrell, and T. Thundat, J. Appl. Phys. **95,** 1162 (2004).

[27] B. J. Davis, P. S. Carney, and R. Bhargava, *Theory of mid-infrared absorption microspectroscopy. I. Homogeneous samples*, Chem. Anal. (submitted 2009).

[28] B. J. Davis, P. S. Carney, and R. Bhargava, *Theory of mid-infrared absorption microspectroscopy. II. Heterogeneous samples*, Chem. Anal. (submitted 2009).

[29] M. Q. Brewster, *Thermal Radiative Transfer And Properties* (Wiley interscience, New York, 1992).

[30] P. G. Datskos, P. I. Oden, T. Thundat, E. A. Wachter, R. J. Warmack, and S. R. Hunter, Appl. Phys. Lett. **69,** 2986 (1996).

# TABLES

TABLE 1. Microcantilever type and properties.

| Cantilever | Type | Substrate Material | $t_s$ $(\mu m)$ | Coating Material | $t_c$ $(nm)$ | L $(\mu m)$ | $L_1$ $(\mu m)$ | w $(\mu m)$ | $2\bar{d}$ $(\mu m)$ |
|---|---|---|---|---|---|---|---|---|---|
| A | Long OTR4-35 (Veeco) | SiN | 0.50 | Au | 60 | 199.0 | 125 | 30.0 | 56.3 |
| B | CSC17/AlBS (Micromasch) | Si | 2.00 | Al | 30 | 461.3 | - | 43.0 | - |
| C | Long OTR8-10 (Veeco) | SiN | 0.70 | Au | 60 | 199.0 | 125 | 30.0 | 56.3 |
| D | Short OTR4-35 (Veeco) | SiN | 0.50 | Au | 60 | 100.0 | 75 | 15.5 | 25.5 |
| E | Short OTR8-10 (Veeco) | SiN | 0.70 | Au | 60 | 100.0 | 75 | 15.5 | 25.5 |
| F | Long CSC11/AlBS (Micromasch) | Si | 1.30 | Al | 30 | 197.6 | 140 | 40.6 | 49.2 |

TABLE 2. Microcantilever response and ranking for an incident wavelength of 7.5 μm

| Cantilever | $\underline{\delta}$ $(pm)$ | | Measured noise $\left(pm/\sqrt{Hz}\right)$ | Predicted noise $\left(pm/\sqrt{Hz}\right)$ | SNR | | Deflection Ranking | SNR Ranking | |
|---|---|---|---|---|---|---|---|---|---|
| | Meas. | Pred. | | | Meas. | Pred. | | Meas. | Pred. |
| A | 127 | 127 | 1.28 | 1.748 | 99.2 | 72.7 | 1 | 3 | 5 |
| B | 114 | 111 | 0.634 | 0.718 | 180 | 155 | 2 | 1 | 1 |
| C | 49.3 | 52.9 | 0.448 | 0.445 | 110 | 119 | 3 | 2 | 3 |
| D | 17.8 | 23.3 | 0.398 | 0.454 | 44.7 | 51.3 | 4 | 5 | 6 |
| E | 11.9 | 9.95 | 0.206 | 0.0810 | 57.8 | 122 | 5 | 4 | 2 |
| F | 9.32 | 9.79 | 0.385 | 0.120 | 24.2 | 81.6 | 6 | 6 | 4 |

# FIGURES

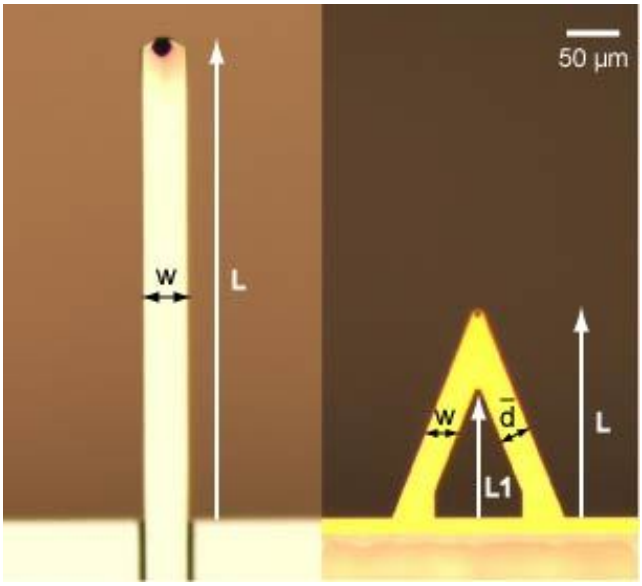


FIGURE 1. Optical microscope pictures of rectangular and V-shaped cantilever used in this study, showing key geometric parameters.

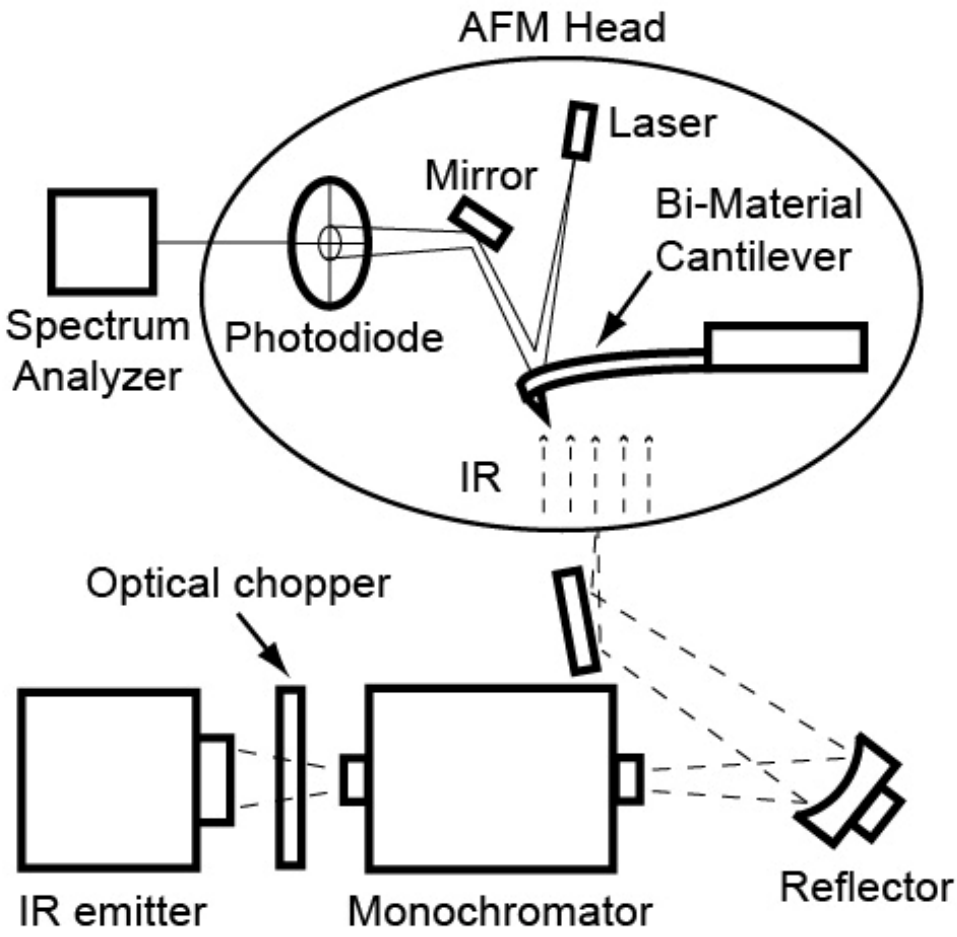


FIGURE 2. Diagram of the experimental setup, where monochromatic infrared beam is incident upon a microcantilever mounted in a commercial atomic force microscope.

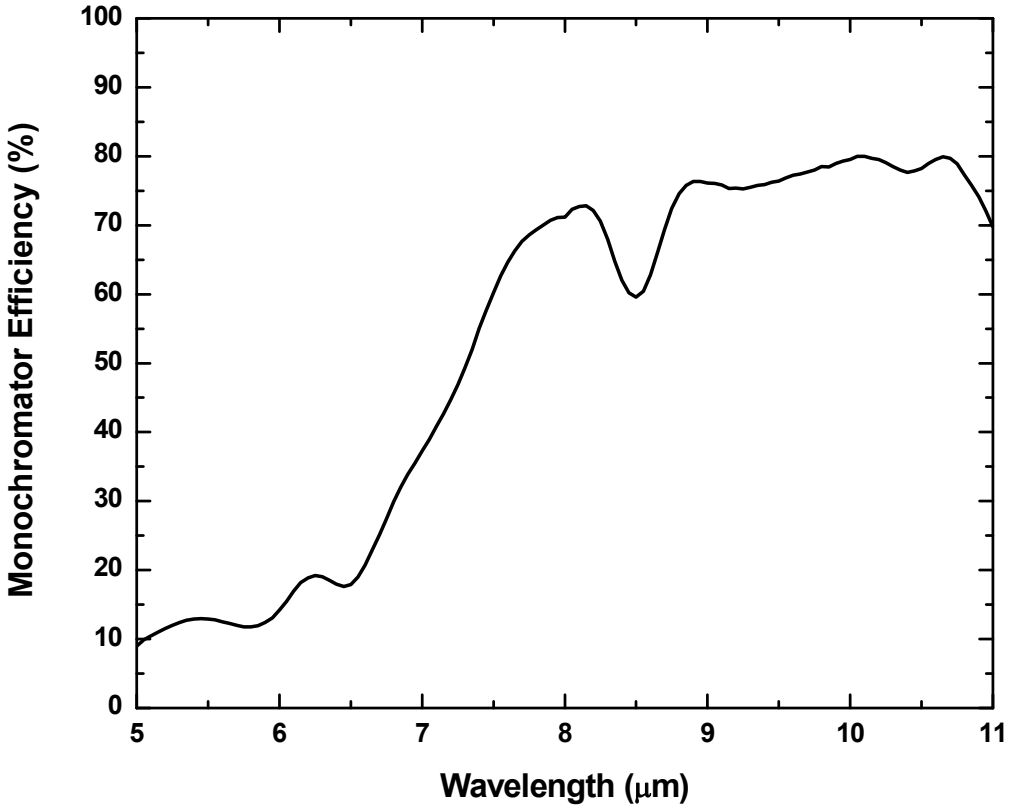


FIGURE 3. Transmission efficiency of the monochromator.

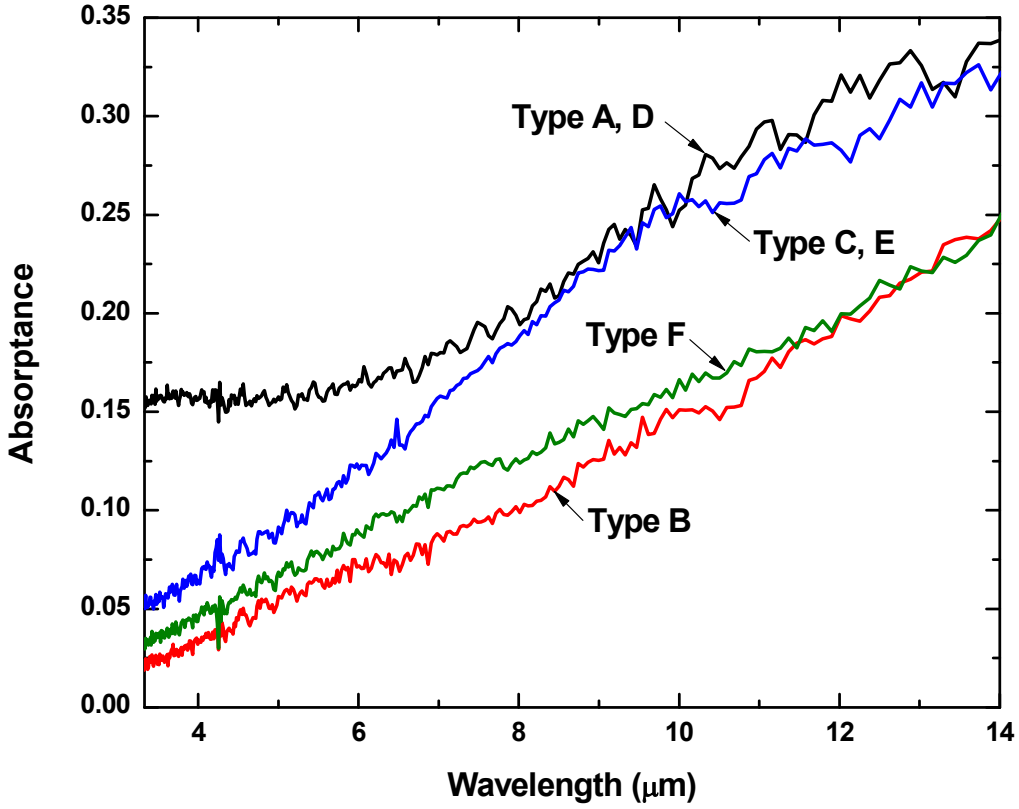


FIGURE 4. The absorption spectra of bimaterial microcantilevers estimated from transmittance and reflectance measurements using a Fourier-transform infrared (FT-IR) spectrometer equipped with a microscope.

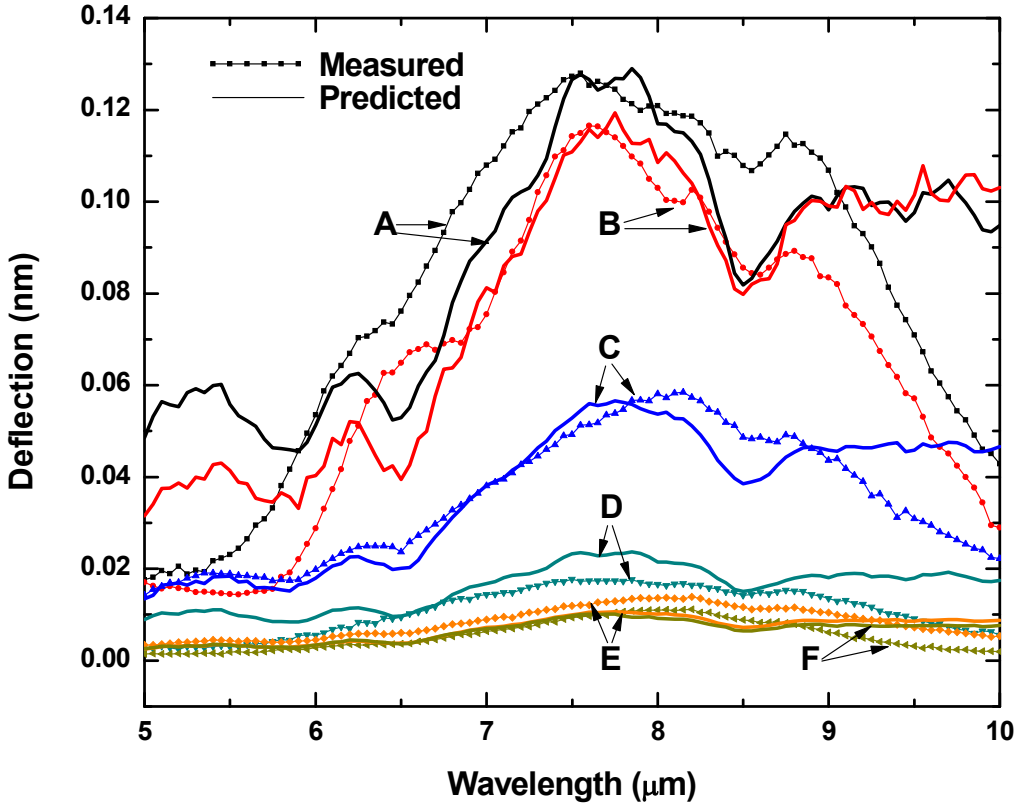


FIGURE 5. Analytical and experimental results of the thermomechanical deflection of the cantilevers under monochromatic infrared illumination in the 5-10 μm bandpass. Solid lines correspond to simulation results and lines with symbols correspond to experimental results.

# APPENDIX A. DERIVATION OF ANALYTICAL SOLUTIONS FOR TEMPERATURE DISTRIBUTION AND THERMOMECHANICAL DEFLECTION OF BIMATERIAL CANTILEVER

When bimaterial cantilever is heated, different thermal expansions of two materials induce thermomechanical deflection of the cantilever as displayed in Figure A.1. The deflection of the bimaterial cantilever can be predicted by solving Eq. (1) when the temperature distribution within the cantilever is known. For the analysis on temperature profile, an arbitrary control volume of the cantilever is taken as shown in Figure A.2. Energy conservation to the control volume can be expressed as,

$$A_1 q_{1(x)} - A_1 q_{1(x+dx)} + A_2 q_{2(x)} - A_2 q_{2(x+dx)} + \frac{P_\lambda}{L} dx - 2(t_1 + t_2 + w)dx \cdot h(T - T_0) = 0 \quad (.4)$$

where $A_1$ and $A_2$ are the cross section areas of two layers, $q_1$ and $q_2$ are conduction heat fluxes across $A_1$ and $A_2$. Introducing Fourier's law gives

$$(A_1 k_1 + A_2 k_2)\frac{d^2 T}{dx^2} + \frac{P_\lambda}{L} - 2(t_1 + t_2 + w)h(T - T_0) = 0 \quad (.5)$$

For mathematical convenience, let $\theta = T - T_0 - \frac{P_\lambda}{2(t_1 + t_2 + w)hL}$ and $\beta^2 = \frac{2(t_1 + t_2 + w)h}{A_1 k_1 + A_2 k_2}$, then the analytical solution of the Eq. (A.2) can be obtained as

$$\theta(x) = B_1 \sinh(\beta x) + B_2 \cosh(\beta x) \quad (.6)$$

At the base of the cantilever ($x = 0$), temperature is assumed to be identical to the ambient temperature $T_0$.

$$\theta(0) = T(0) - T_0 - \frac{P_\lambda}{2(t_1 + t_2 + w)hL} = -\frac{P_\lambda}{2(t_1 + t_2 + w)hL} \quad (.7)$$

At the free end of the cantilever ($x = L$), the heat loss is tiny and can be ignored in many cases due to small cross section area of the cantilever. Thus,

$$\left.\frac{dT}{dx}\right|_{x=L} = \left.\frac{d\theta}{dx}\right|_{x=L} \simeq 0 \qquad (.8)$$

Using these two boundary conditions, $B_1$ and $B_2$ can be solved as

$$B_1 = \frac{P_\lambda}{2(t_1 + t_2 + w)hL}\tanh(\beta L)$$

$$B_2 = -\frac{P_\lambda}{2(t_1 + t_2 + w)hL}$$

Substituting $B_1$ and $B_2$ in Eq. (A.3) and rearranging gives the temperature distribution as

$$T(x) - T_0 = \frac{P}{2(t_1 + t_2 + w)hL}\left[\tanh(\beta L)\sinh(\beta x) - \cosh(\beta x) + 1\right] \qquad (.9)$$

With $T(x) - T_0$ obtained from Eq. (A.6), now Eq. (1) can be rewritten as

$$\frac{d^2 z}{dx^2} = 3(\alpha_1 - \alpha_2)\left(\frac{t_1 + t_2}{{t_2}^2 K}\right)\frac{P}{(t_1 + t_2 + w)hL}(\tanh(\beta L)\sinh(\beta x) - \cosh(\beta x) + 1) \qquad (.10)$$

Eq. (A.7) has the solution

$$z(x) = 3(\alpha_1 - \alpha_2)\left(\frac{t_1 + t_2}{{t_2}^2 K}\right)\frac{P}{(t_1 + t_2 + w)hL}\left[\frac{\tanh(\beta L)\sinh(\beta x)}{\beta^2} - \frac{\cosh(\beta x)}{\beta^2} + \frac{x^2}{2} + C_1 x + C_2\right] \qquad (.11)$$

Because both the deflection and the slope at the base of cantilever ($x = 0$) are 0, unknown constants $C_1$ and $C_2$ can be obtained as

$$C_1 = -\frac{\tanh(\beta L)}{\beta}$$

$$C_2 = \frac{1}{\beta^2}$$

Substituting $C_1$ and $C_2$ in Eq. (A.8) gives the thermodeflection of cantilever as

$$z(x) = 3(\alpha_1 - \alpha_2)\left(\frac{t_1 + t_2}{{t_2}^2 K}\right)\frac{P}{(t_1 + t_2 + w)hL\beta^2}\left(\tanh(\beta L)\left(\sinh(\beta x) - \beta x\right) - \cosh(\beta x) + \frac{1}{2}\beta^2 x^2 + 1\right)$$

( .12)

Then using Eq. (A.9), the analytical solution for cantilever deflection at the free end can be readily predicted as Eq. (2).

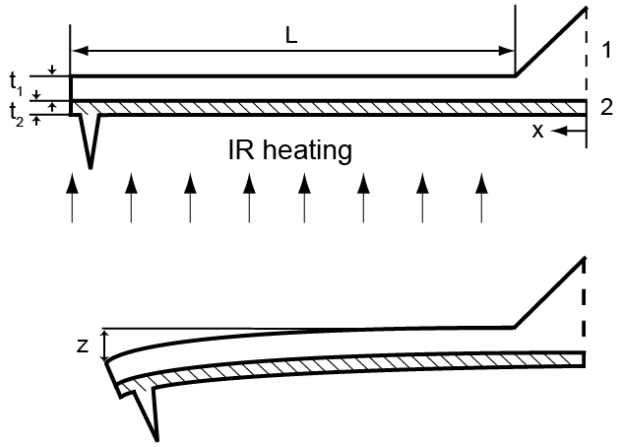


FIGURE A.1. Schematic of bimaterial cantilever deflection induced by IR heating.

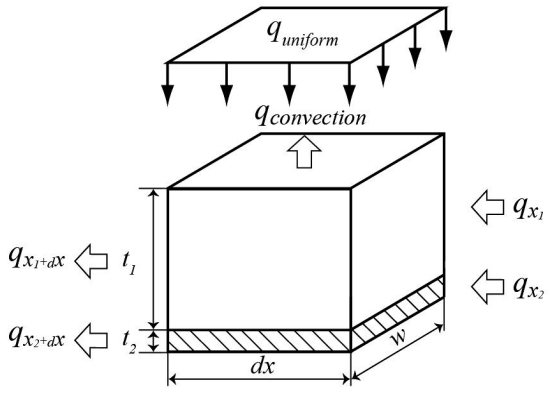


FIGURE A.2. An elemental control volume of cantilever for application of the energy conservation principle.

# APPENDIX B. CALCULATION OF THERMOMECHANICAL DEFLECTION OF TYPE A CANTILEVER WITH MATLAB

## B.1. Main source code

```
% This program will calculate the thermomechanical bending of type A
% microcantilever upon infrared heating over 5-10um range. The calculation
% is estimated from incident IR radiation, IR response characteristics of
% the cantilever, and the mechanical properties of the cantilever. To
% evaluate the thermomechanical bending of different type cantilever,
% different mechanical and IR absorption properties of the cantilever are
% needed to be applied.

%%%%%%%%%%%%%%%%%%%%%%%%%%%%%%%%%%%%%%%%%%%%%%%%%%%%%%%%%%%%%%%%%%%%%%%%%%%
%% Material Properties and Geometry of Cantilever
%%%%%%%%%%%%%%%%%%%%%%%%%%%%%%%%%%%%%%%%%%%%%%%%%%%%%%%%%%%%%%%%%%%%%%%%%%%

% Properties of cantilever components
% Data are obtained from online data base (www.Matweb.com). Depending on
% the type of cantilever, specific values should be modified.
a1 = 2.8e-6;                % Thermal expension coefficient of SiNx [1/K]
a2 = 14.4e-6;               % Thermal expension coefficient of Au [1/K]
E1 = 290e9;                 % Young's modulus of SiNx [Pa]
E2 = 77.2e9;                % Young's modulus of Au [Pa]
k1 = 16;                    % Thermal conductivity of SiNx at 300K [W/m-K]
k2 = 301;                   % Thermal conductivity of Au at 300K [W/m-K]
phi = E1/E2;                % Ratio of Young's modulus
```

```
% Cantilever geometry
L = 125e-6;                 % Equivalent length of type A cantilever [m]
t1 = 0.5e-6;                % SiNx thickness of type A cantilever [m]
t2 = 60e-9;                 % Au thickness of type A cantilever [m]
wd = 2*28.16877e-6;         % Equivalent width of type A cantilever [m]
A1 = t1*wd;                 % Cross-section area of SiNx layer [m^2]
A2 = t2*wd;                 % Cross-section area of Au layer [m^2]
n = t1/t2;                  % Ratio of thickness

%%%%%%%%%%%%%%%%%%%%%%%%%%%%%%%%%%%%%%%%%%%%%%%%%%%%%%%%%%%%%%%%%%%%%%%%%%%%%%%
%% Calculation of Spectral Irradiation on Cantilever
%%%%%%%%%%%%%%%%%%%%%%%%%%%%%%%%%%%%%%%%%%%%%%%%%%%%%%%%%%%%%%%%%%%%%%%%%%%%%%%

% Spectral region of interest
lambda = [5:0.05:10];               % Wavelength [um]

% Emission from IR emitter
% Graybody spectral radiation predicted by Planck's function
Q = Radiation(lambda);              % Spectral radiant power [W/um]

% Reflected radiation from a grating of monochromator
% To apply monochromator efficiency
Q = Grating_efficiency_Meas_GE(Q);  % Spectral radiant power [W/um]

% Irradiation on cantilever
eta_m = 0.95;                       % Average mirror (AlMgF2) reflectivity
                                    % to mid-infrared radiation
dA = 245e-6;                        % Focal area [m^2]
```

```
I = Q*eta_m^6/dA;                    % Irradiation intensity [W/m^2-um]
                                     % 6 mirrors exist along the light path.

%%%%%%%%%%%%%%%%%%%%%%%%%%%%%%%%%%%%%%%%%%%%%%%%%%%%%%%%%%%%%%%%%%%%%%%%%%%%
%% Calculation of Absorbed Radiant Power
%%%%%%%%%%%%%%%%%%%%%%%%%%%%%%%%%%%%%%%%%%%%%%%%%%%%%%%%%%%%%%%%%%%%%%%%%%%%

I = abs_coeff_OTR4(I);               % Absorbed irradiation intensity [W/m^2
                                     % -um]
P_uniform = I*9953.05E-12;           % Absorbed radiant power [W/um]
                                     % Area of cantilever is estimated to be
                                     % 9953.05E-12 m^2

%%%%%%%%%%%%%%%%%%%%%%%%%%%%%%%%%%%%%%%%%%%%%%%%%%%%%%%%%%%%%%%%%%%%%%%%%%%%
%% Temperature Distribution and Thermal Bending of Cantilever
%%%%%%%%%%%%%%%%%%%%%%%%%%%%%%%%%%%%%%%%%%%%%%%%%%%%%%%%%%%%%%%%%%%%%%%%%%%%

h = 1000;                          % Air conduction transfer coeff [W/m^2-K]
beta = sqrt(2*(t1+t2+wd)*h/(A1*k1+A2*k2));  % A parameter for calculation
K = 4 + 6*n + 4*n^2 + phi*n^3 + 1/(phi*n);  % A parameter for calculation
x = linspace(0,L,50)';             % Position of nodes

% Analytical soltion for temperature distribution and thermal bending

for i = 1:length(P_uniform)

    % Distribution of temperature difference between the cantilever and amb
```

```
    % ient air along cantilever predicted by the relation introduced in App
    % endix A.
    T = P_uniform(i)*(tanh(beta*L)*sinh(beta*x)-cosh(beta*x)+1)/...
        (2*(wd+t1+t2)*h*L);          % T-T0 [K]

    % Deflection of cantilever from its neutral position at different nodal
    % position predicted by the relation introduced in Appendix A.
    z = -3*(a1-a2)*((t1+t2)/(t2^2*K))*(P_uniform(i)/((t1+t2+wd)...
        *h*L))*(tanh(beta*L)*(sinh(beta*x)-beta*x)/beta^2 - (cosh(beta*...
        x)-1)/beta^2 + 0.5*x.^2);    % Deflection [m]

    % Deflection of cantilever from its neutral position at the free end of
    % cantilever predicted by the relation introduced in Appendix A.
    z_free_end(i,1) = z(50)*1e9;    % Maximum deflection [nm]
end
```

## B.2. **Subroutines** for main source code

### B.2.1. Radiation( )

```
function [Q] = Radiation(lambda)
% This program will predict the emitted radiant power of IR emitter from
% Planck's equation. View factor and temperature of globar should be
% modified for different optical setting.

% Physical constants
c0 = 2.99792458e+8;          % Speed of light [m/s]
hh = 6.6260689633e-34;       % Planck's constant [J-s]
k = 1.3806503e-23;           % Boltzmann's constant [J/K]

% Optical setup configuration
d_s = 6.7e-3;                % Globar diameter [m]
L_s = 89e-3;                 % Globar length [m]
% L_m = 46e-3;                % Mirror length [m]
% A_m = L_m^2;                % Mirror area [m^2]
% S_ms = 132.5e-3;            % Distance btw mirror and globar [m]
% X_ms = 45e-3;               % X-distance btw mirror and globar [m]
% Y_ms = sqrt(S_ms^2-X_ms^2);% Y-distance btw mirror and globar [m]

% Globar
A_gb = pi*d_s*L_s;           % The cross-section area of the globar [m^2]
F = 0.05;                    % View factor obtained from 'F.P.Incropera and
                             % D.P.DeWitt, Fundamentals of Heat and Mass
```

```
                            % Transfer, 5th ed., John Wiley & Sons, New
                            % Jersey, 2002.'
T_gb = 1100;                % Temperature [K]

% Calculation of emitted radiant power of IR emitter
I_b = ((2*hh*c0^2./((lambda*1e-6).^5.*(exp(hh*c0./((lambda*1e-6)*k*T_gb...
    ))-1)))*1e-6)';         % Spectral blackbody intensity predicted by
                            % Planck's equation [W/(m^2-Sr-um)]
I_b = Emissivity(I_b);      % Spectral graybody intensity by applying
                            % emissivity of globar provided by the vendor
Q = A_gb*F*I_b;             % Emission from the IR emitter [W/um]
```

### B.2.1.1. Subroutine for Radiation( ), Emissivity( )

```
function [I_b] = Emissivity(I_b)
% This code will generate emissivity values at wavelengths of interest
% using curve fitting technique. Emissivity curve is obtained from the
% globar manufacturer and fitted in second order polynomial. Emissivity
% will be used to calculate spectral graybody intensity by multiplying to
% predicted blackbody intensity of the IR emitter.

% Spectral region of interest
lambda1 = [5:0.05:8.65];    % First spectral region for curve fitting [um]
lambda2 = [8.675:0.05:10];  % Second spectral region for curve fitting [um]
lambda = [lambda1 lambda2]; % Entire spectral region of interest [um]
```

```
% Curve fitted emissivity using second order polynomials
emissivity1 = 0.53454 + 0.12504*lambda1 - 0.01307*lambda1.^2;
    % Curve fitting for the first spectral region using emissivity curve
    % from the vendor.
emissivity2 = -5.81959 + 1.28149*lambda2 - 0.06215*lambda2.^2;
    % Curve fitting for the second spectral region using emissivity curve
    % from the vendor.
emissivity2(1:2) = [0.6350 0.6325]; % Correction on curve fitting
emissivity_fit = [emissivity1 emissivity2]';
    % Curve fitting for the entire spectral region of interest

% Calculation of spectral graybody intensity
I_b = emissivity_fit.*I_b;  % [W/(m^2-Sr-um)]
```

### B.2.2. Grating_efficiency_Meas_GE( )

```
function [Q] = Grating_efficiency_Meas(Q)
% This code will produce grating efficiency values at wavelengths of
% interest using interpolation technique. Grating efficiency was measured
% using FT-IR spectrometer and will be interpolated. This efficiency will
% be used to estimate the radiant power reflected off grating.

% Load grating efficiency measurement data
temp = load('Grating_efficiency_meas.txt');
x = temp(:,1);  % Wavelength region used for grating efficiency measurement
y = temp(:,2);  % Grating efficiency
```

```
% Interpolation of measurement data at wavelengths used in main source code
lambda = 5:0.05:10;      % Wavelengths used in main source code [um]
eta_g = interp1(x,y,lambda,'cubic');     % Interpolation of measurement data

% Calculation of the radiant power reflected off grating
Q = Q.*eta_g';  % [W/um]
```

### B.2.3. abs_coeff_OTR4( )

```
function [Q] = abs_coeff_OTR4(Q)
% This code will create absorptivity of type A cantilever at wavelengths of
% interest using interpolation technique. Absorptivity was measured using
% FT-IR spectrometer and will be interpolated. This absorptivity will be
% utilized to predict the absorbed radiant power.

% Load the measurement data of absorptivity of type A cantilever
temp = load('Absorptivity_OTR4.txt');
x = temp(:,1);  % Wavelength region used for grating efficiency measurement
y = temp(:,2);  % Absorptivity

% Interpolation of measurement data at wavelengths used in main source code
lambda = 5:0.05:10;          % Wavelengths used in main source code [um]
abs_coeff = interp1(x,y,lambda,'cubic');% Interpolation of measurement data

% Calculation of absorbed radiant power
Q = Q.*abs_coeff';  % [W/um]
```

# APPENDIX C. CALIBRATION OF CANTILEVER DETECTOR DEFLECTION VOLTAGE TO DEFLECTION DISTANCE

AFM optical readout system consists of a solid state diode and a position sensitive detector (PSD) which is composed of two closely spaced photodiodes. The solid state diode illuminates laser of 670 nm wavelength on the surface of cantilever which will be reflected to PSD. Depending on the angular displacement of cantilever, different amount of laser is absorbed by each photodiode in PSD. Based on the difference between the absorption, PSD generates voltage signal which can be translated into the deflection distance by being multiplied by deflection sensitivity of cantilever. Deflection sensitivities of cantilevers used in this study are measured as shown in the table C.1 from force spectroscopy which shows the PSD deflection voltage as a function of the vertical movement of the piezoelectric transducer when cantilever contacts rigid surface such as mica. The inverse of the slope of the contact portion of the spectroscopy is the deflection sensitivity of the cantilever.

TABLE C.1. Deflection sensitivities of cantilevers

| Type of cantilever | A | B | C | D | E | F |
|---|---|---|---|---|---|---|
| Deflection Sensitivity [nm/V] | 143 | 171 | 115 | 60.3 | 52.3 | 115 |